# LANGMUIR

pubs.acs.org/Langmuir Article

# Investigation of Cell Aggregation on the Printing Performance in Inkjet-Based Bioprinting of Cell-Laden Bioink

Heqi Xu, Jiachen Liu, Md Shahriar, and Changxue Xu\*



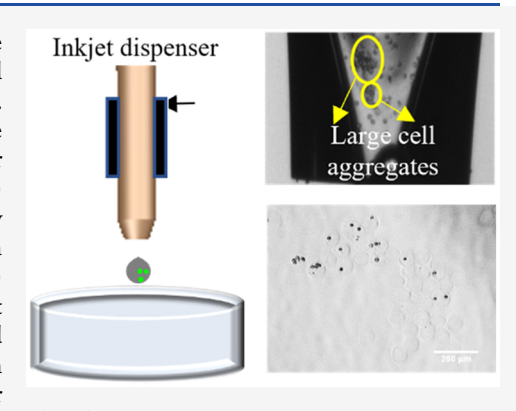
Cite This: Langmuir 2023, 39, 545-555



**ACCESS** I

Metrics & More

ABSTRACT: During 3D bioprinting, when the gravitational force exceeds the buoyant force, cell sedimentation will be induced, resulting in local cell concentration change and cell aggregation which affect the printing performance. This paper aims at studying and quantifying cell aggregation and its effects on the droplet formation process during inkjet-based bioprinting and cell distribution after inkjet-based bioprinting. The major conclusions of this study are as follows: (1) Cell aggregation is a significant challenge during inkjet-based bioprinting by observing the percentage of individual cells after different printing times. In addition, as polymer concentration increases, the cell aggregation is suppressed. (2) As printing time and cell aggregation increase, the ligament length and droplet velocity generally decrease first and then increase due to the initial increase and subsequent decrease of the viscous effect. (3) As the printing time increases, both the maximum number of cells within one microsphere and the mean cell number



Article Recommendations

have a significant increase, especially for low polymer concentrations such as 0.5% (w/v). In addition, the increased rate is the highest using the lowest polymer concentration of 0.5% (w/v) because of its highest cell sedimentation velocity.

### 1. INTRODUCTION AND BACKGROUND

Recently, 3D bioprinting has been broadly recognized as a promising solution for the fabrication of native-like tissues and organs based on depositing the cell-laden bioink layer-bylayer. 1,2 Typically, bioprinting techniques can be classified into inkjet-based bioprinting, microextrusion-based bioprinting, laser-assisted bioprinting, and stereolithography-based bioprinting.<sup>3</sup> During inkjet-based bioprinting, with the implementation of either a heating element or a piezoelectric actuator, cell-laden droplets are ejected out of the nozzle and deposited onto a substrate.4 Inkjet-based bioprinting is favored for its high deposition accuracy, printing resolution, and cell viability. However, high polymer and cell concentrations are not applicable due to high viscosity.<sup>6</sup> Microextrusion-based bioprinting enables the generation of a continuous filament through a microextruder. Despite its large allowance on the polymer and cell concentrations, low cell viability and printing speed hinder its wide applications. 9 Benefiting from the nozzlefree mechanism, laser-assisted bioprinting is capable of precisely ejecting the bioink with high polymer and cell concentrations<sup>10</sup> through laser-induced bubble expansion.<sup>11</sup> However, the applications of laser-assisted bioprinting is limited by its high cost<sup>4</sup> and probable metallic contamination. 12 Stereolithography-based bioprinting uses either visible light or ultraviolet (UV) light to polymerize photosensitive materials into 3D structures layer by layer. 13 One significant limitation is that the materials used in stereolithography are restricted to photopolymers. <sup>14,15</sup> Inkjet-based bioprinting holds attributes such as high precision and accurate controllability of the deposition of the bioink. 16 Thus, inkjetbased bioprinting is selected in this study. Typically, inkjetbased bioprinting has been selected to print a variety of biomaterials (e.g., alginate<sup>17</sup> and polyethylene glycol (PEG)<sup>18</sup>) and living cells (e.g., endothelial cells (ECs)19 and human umbilical vein endothelial cells (HUVECs)20). Inkjet-based bioprinting has already artificially created several tissues/ organs, such as bone,<sup>21</sup> skin,<sup>22</sup> and cartilage.<sup>23</sup> For example, Gao et al. selected inkjet-based bioprinting to create bone and cartilage scaffolds composed of polyethylene glycol diacrylate (PEGDA), gelatin methacrylate (GelMA), and bone marrow derived human mesenchymal stem cells (hMSCs).<sup>21</sup> Xu et al. selected inkjet-based bioprinting to successfully fabricate vascular-like constructs with both vertical and horizontal configurations.<sup>24</sup> Jiao et al. inkjet-printed the bioink with a dual-step cross-linking mechanism into soft tissues with enhanced mechanical properties demonstrating the feasibility of inkjet-based bioprinting for the fabrication of native tissues.2

Received: October 14, 2022 Revised: December 6, 2022 Published: December 23, 2022





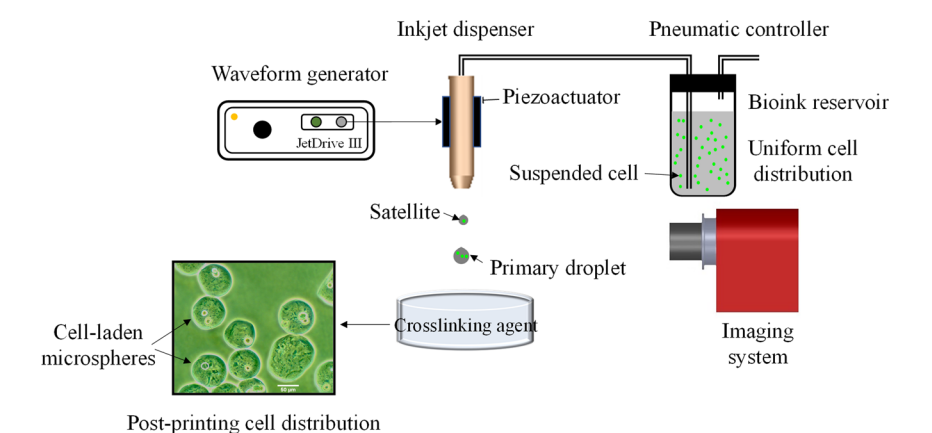


Figure 1. Schematic diagram of inkjet-based bioprinting.

As a key element in 3D bioprinting, bioink typically contains biological materials whose function is to mimic natural extracellular matrix (ECM) promoting cellular activities such as cell proliferation and differentiation 26,27 and living cells. Suitable biomaterials should possess good printability, biocompatibility, and biodegradability. <sup>28–30</sup> A variety of biomaterials including naturally derived polymers (e.g., collagen<sup>31</sup> and alginate<sup>32</sup>) and synthetic polymers (e.g., hyaluronic acid methacrylate (HAMA)<sup>33</sup> and polylactide (PLA)<sup>34</sup>) have been broadly selected for 3D bioprinting. Meanwhile, a variety of cells have also been printed, such as mesenchymal stem cells (MSCs)<sup>35</sup> and human pluripotent stem cells (hiPSCs).<sup>36</sup> One significant challenge in inkjet printing is to maintain the uniformity of the cell distribution within the low-viscosity bioink, which is of great significance to the printing reliability of artificial functional tissues/organs.<sup>3</sup> When the gravitational force dominates the buoyant force, cells continuously sediment. The cell sedimentation results in nonuniformity of the cell distribution with a lower cell concentration on the top and a higher cell concentration at the bottom of the bioink reservoir. When adjacent cells become close to each other, cell aggregates are facilitated to form due to the cell-cell interaction force. The nonuniformity of the cell concentration and cell aggregates significantly influence the rheological properties (e.g., viscosity and viscoelasticity) of the bioink<sup>38</sup> as well as the corresponding printing reliability. In this paper, the printing reliability is quantified using the droplet formation process, and the printing quality focuses on the postprinting cell distribution representing the cell number within the formed microspheres.

In the literature, several papers reported the cell sedimentation and aggregation as well as the associated adverse effects on the printing performance during 3D bioprinting of the low-viscosity bioink.<sup>39</sup> For example, Saunders et al.<sup>40</sup> inkjet-printed human fibroblast (HT1080 fibrosarcoma). A significant reduction of the cell concentration in the bioink reservoir was reported after 20 min of printing due to the cell sedimentation and aggregation. Parsa et al.4 reported inconsistent printing results in inkjet bioprinting of the bioink with Hep G2 hepatocytes. Despite a frequent stirring (5 s for every 2 min printing) within the bioink reservoir, cell sedimentation and the resulting cell aggregation still resulted in a large variation in the printed cell number. In a recent study presented by Chahal et al., 42 the sedimentation velocity of MCF-7 breast cancer cells in the bioink containing cell culture medium was measured to be 7.5  $\mu$ m/s. Cell

aggregation resulted in a highly nonuniform cell number per well from around 300-5000 cells per well. Graham et al. 43 reported a significant increase in the suspended ovine mesenchymal stem cells (oMSCs) concentration within the bioink due to cell sedimentation. The highest cell concentration was reported to be around  $3 \times 10^7$  cells/mL, which was nearly three times that of the initial cell centration. In a recent study, Xu et al.<sup>44</sup> analyzed the force imposed on a single cell during cell sedimentation and presented a comprehensive study on the cell sedimentation velocity and the resulting cell concentration change using different polymer concentrations and at different printing times. It was reported that the cell sedimentation velocity was between 0 and 1.5  $\mu$ m/s, and the bottom cell concentration within the bioink reservoir could be 4 times higher after 2 h of printing. Moreover, cell aggregation was observed using 0.5% (w/v) sodium alginate at 120 min printing time. Recently, Xu et al. 45 investigated the effect of cell sedimentation on the cell concentration and cell aggregation within the bioink reservoir. It was reported that only within 40 min of printing time, almost all of the cells within the bioink containing 0.5% (w/v) sodium alginate have sedimented to the bottom, significantly increasing the cell concentration and facilitating cell aggregation. Later, the same group presented a study characterizing cell aggregation both during and after the inkjet-based bioprinting process.<sup>46</sup> It was observed that the percentage of cells forming cell aggregates at the bottom of the bioink reservoir increased significantly from 3.6% to 54.5% within 60 min of printing time. In addition, a huge percentage of cells have been found to adhere to form cell aggregates both within the inkjet nozzle during printing and formed microspheres after printing. In summary, the cell aggregation due to the cell sedimentation is a crucial problem in inkjet-based bioprinting. Therefore, it is critical to understand the physics behind the cell aggregation and its effect on the printing performance in the inkjet-based bioprinting.

Although the cell aggregation phenomenon due to the cell sedimentation has been reported in the literature, there is no published work regarding the physical understanding of the cell aggregation and the associated effects on the printing performance during inkjet-based bioprinting. This paper is the first study to answer two fundamental questions regarding the physics of the cell aggregation phenomenon: (1) how to quantify the cell aggregation in inkjet-based bioprinting and (2) how the cell aggregation affects the printing performance relating to the droplet formation process and postprinting cell distribution. The organization of the remaining sections is as

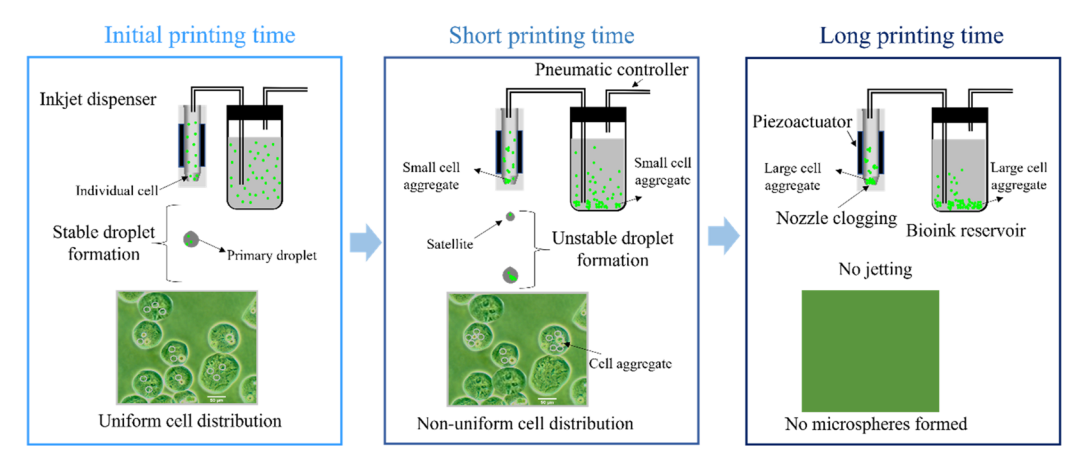


Figure 2. Cell aggregation phenomenon with the printing time and its significant consequences on the printing reliability and postprinting quality in inkjet-based bioprinting.

follows: section 2 presents the bioink preparation, experimental conditions, and cell aggregation characterization; section 3 characterizes the cell aggregation within the nozzle at different printing times and further investigates how the cell sedimentation-induced cell aggregation affects the droplet formation process during inkjet printing and the postprinting cell distribution; and section 4 draws the major conclusions and proposes future work.

# 2. MATERIALS AND METHODS

**2.1. Bioink Preparation.** As a key element in 3D bioprinting, bioink mainly contains biomaterials and living cells. <sup>47</sup> Sodium alginate which is a hydrogel with exceptional biocompatibility <sup>48</sup> was used in this study to mimic natural ECM allowing cell attachment, proliferation, and differentiation. NIH 3T3 mouse fibroblasts as a common cell type in connective tissues <sup>49,50</sup> were selected in this study. The bioink was prepared as follows: (1) Mix sodium alginate powder (Sigma-Aldrich, St. Louis, MO) within Dulbecco's Modified Eagles Medium (DMEM; Sigma-Aldrich, St. Louis, MO) to prepare 0.5%, 1%, and 1.5% (w/v) DMEM-based sodium alginate solutions; (2) collect the cell pellet from the culturing flask (Fisher Scientific, Pittsburgh, PA) after 5 min of centrifuging; and (3) resuspend the collected cell pellet into the prepared sodium alginate solutions for a  $1.5 \times 10^6$  cells/mL cell concentration. More details can refer to our previous papers. <sup>51–53</sup>

2.2. Experimental Setup. Figure 1 schematically shows our inkjet-based bioprinting system. Typically, the system is composed of a piezoactuator-based inkjet nozzle, a small reservoir containing the bioink, a pneumatic controller, a waveform generator, a horizontal imaging system (jetXpert, Nashua, NH), and a substrate containing 2% (w/v) calcium chloride to receive and cross-link the cell-laden droplets in this study. The function of the pneumatic controller was to maintain the back pressure between -14 and -12 kPa to ensure a flat meniscus at the nozzle tip during the droplet formation process. The horizontal imaging system captured the real-time images of the cell movement inside the nozzle and the droplet formation process. A bipolar waveform was imposed on the piezoelectric actuator to deform the inkjet nozzle and eject cell-laden droplets. The bioink inside the inkjet nozzle was ejected out from the nozzle orifice to form a ligament which broke up into one or several cell-laden droplets. The droplet formation process is dependent on not only the processrelated parameters (e.g., the excitation voltage) but also the materialsrelated parameters (e.g., the polymer and cell concentration). And postprinting cell distribution varies and depends on the operating conditions in the droplet formation process.

Figure 2 representatively shows the cell aggregation phenomenon due to the cell sedimentation and the corresponding consequences on the printing performance of inkjet-based bioprinting. Initially, the cells

are uniformly suspended in the bioink, and the individual cells are separate from each other, indicating a uniform cell distribution within the bioink reservoir. The droplet formation process is reliable, resulting in relatively uniform postprinting cell distribution within the microspheres. 50,51 However, due to cell sedimentation, the bottom cell concentration is significantly increased. Once the cells are closer, the formation of cell aggregates is facilitated due to the cell-cell interaction force. The cell aggregation is critical to the rheological properties of the bioink (e.g., viscoelasticity), which significantly influences the subsequent droplet formation process and postprinting cell distribution. Specifically, the droplet formation process becomes unstable in terms of the ligament length, breakup time, droplet size, and velocity. The postprinting cell distribution becomes highly nonuniform. Most microspheres formed contain no cells. At long printing times, the cell aggregation problem is more severe. More and more cells aggregate with each other, and the formed cell aggregates become larger and larger. When the size of the cell aggregates is comparable to the size of the inkjet dispenser orifice (e.g., 120  $\mu$ m in this study), a nozzle clogging phenomenon is observed, and no droplets or microspheres are formed. Figure 2 summarizes the cell aggregation phenomenon with the printing time and its significant consequences in the printing reliability and postprinting quality.

2.3. Characterization and Conditions. Inkjet-based bioprinting has been intensively utilized in various biomedical applications.<sup>5</sup> Recently, the droplet formation process and postprinting quality during inkjet bioprinting have been studied. 50,55 However, the study focusing on the cell aggregation in inkjet-based bioprinting is still missing. The cell aggregation phenomenon is a significant challenge in inkjet-based bioprinting because of its critical effects on the printing reliability as well as postprinting quality. Hence, it is critical to understand the cell aggregation phenomenon in inkjet-based bioprinting. Our paper is the first study to tackle this problem. In this section, we elaborate how to quantify the cell aggregation in inkjet-based bioprinting. During inkjet-based bioprinting, the cells have three existing forms, including individual cells without aggregation, small cell aggregates composed of two to four cells, and large cell aggregates composed of at least five cells. The percentage of individual cells, small cell aggregates, and large cell aggregates was characterized as

ic % = 
$$\frac{\sum_{a=1} ab}{\text{Totl number of cells}} \times 100\%$$
, sa %
$$= \frac{\sum_{a=2}^{4} ab}{\text{Total number of cells}} \times 100\%$$
, and la %
$$= \frac{\sum_{a=5}^{6} ab}{\text{Total number of cells}} \times 100\%$$

respectively, where a refers to the number of cells forming cell aggregates (a is 1 for individual cells), b refers to the appearance

frequency of individual cells and cell aggregates, and c refers to the number of cells constituting the largest cell aggregates. The droplet formation process was characterized in terms of the ligament length, breakup time, and droplet velocity. 50 The ligament length refers to the distance between the nozzle orifice and the first pinch-off location; the breakup time is defined as the needed time for the first pinch-off, and the droplet velocity is calculated by dividing the ligament length by the breakup time. In addition, the postprinting quality was characterized using the cell distribution within the microspheres. A total of 1000 random microspheres were chosen under each condition, and the average number of cells within one microsphere was calculated using  $\mu = \sum_{x=0}^{n} xy$ , where x represents the cell number within one microsphere, y represents the associated appearance percentage, and n represents the largest number of cells within one microsphere. In this study, three commonly used sodium alginate concentrations, 0.5%, 1%, and 1.5% (w/v), were selected to avoid nozzle clogging and ensure continuous jetting. 56 concentration was  $1.5 \times 10^6$  cells/mL. The printing was controlled within a 15 min printing time, and the printing quality was checked every 5 min.

# 3. RESULTS AND DISCUSSIONS

During the printing process, the buoyant force is always unable to balance the gravitational force, resulting in cell sedimentation.<sup>39</sup> As reported by Xu et al., the bottom cell concentration within the bioink reservoir increases continuously and significantly because of cell sedimentation.<sup>44</sup> Once the cells become close enough, the cell-cell interaction force becomes significant and drives the cells to adhere and form different sizes of cell aggregates.<sup>59</sup> The formation of cell aggregates induced by the cell sedimentation has a significant effect on the printing reliability. This study mainly studies the cell aggregation and its effects on the droplet formation process during inkjet bioprinting and postprinting cell distribution. Specifically, section 3.1 investigates how the cell aggregates within the nozzle are gradually formed with the printing time during the droplet formation process. The percentages of individual cells, small cell aggregates, and large cell aggregates as previously mentioned are quantified at different printing times. Section 3.2 focuses on how cell aggregation affects the droplet formation process by studying the changes in ligament length, breakup time, and droplet velocity at different printing times. Section 3.3 investigates how the cell aggregation affects the postprinting cell distribution at different printing times.

3.1. Effect of Printing Time on Cell Aggregation inside the Nozzle. Figure 3 shows the formation process of the cell aggregates with printing time during inkjet printing of the bioink containing 0.5% (w/v) sodium alginate and 1.5  $\times$ 10<sup>6</sup> cells/mL cell concentration. It was reported that the cell sedimentation velocity with this polymer concentration is around 1.45  $\mu$ m/s.<sup>44</sup> At 0 min printing time, the cells are uniformly suspended in the bioink. The cells are separate from each other, and the cell concentration is uniform. At 5 min printing time, the cell sediments to the bottom, and the local cell concentration increases significantly. It is observed that the cells start to form small aggregates containing two or three cells. At 15 min printing time, the distance between the cells becomes very close, facilitating the further aggregation. It was observed that the cells formed large aggregates containing even more than 10 cells. And this number increases to around 30 cells at 30 min printing time. At 45 min printing time, the cell aggregate size is comparable to the nozzle orifice size, and the nozzle is blocked with no jetting and droplets generated. It is noted that Figure 3 is a representative figure of the cell aggregate formation during inkjet-based bioprinting using 0.5%

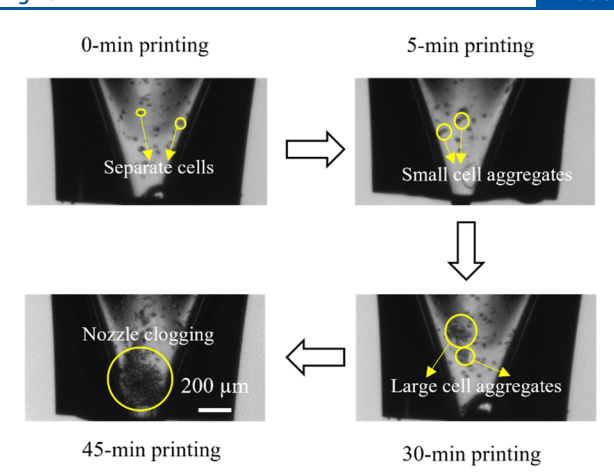


Figure 3. Formation process of cell aggregates with the printing time. The bioink contains 0.5% (w/v) sodium alginate and a cell concentration of  $1.5\times10^6$  cells/mL.

(w/v) sodium alginate-based bioink. Adjustment of the operating conditions may accelerate or delay the cell aggregation formation process. For instance, for the bioink containing 1% (w/v) sodium alginate, the nozzle blockage was not observed within a 60 min printing time due to the slower cell sedimentation process.

Figure 4 shows the change in the cell aggregation percentage with the printing time at different sodium alginate concentrations. At 0 min, the bioink is uniform without cell aggregation with 100% individual cells and 0% cell aggregates. During printing, the suspended cells continuously sediment to increase the bottom cell concentration, resulting in formation of the cell aggregates. The cell concentration within the nozzle is not uniform. Due to the cell sedimentation, the cell concentration is low at the top and high at the bottom. At a short printing time, the majority of the cells form small aggregates inside the nozzle, and the large aggregates are formed at the very bottom of the nozzle due to relatively high cell concentration. With the printing time, the percentage of the individual cells and cell aggregates decreases and increases significantly, respectively. For example, as the printing time increases from 0 to 5 to 10 to 15 min, the percentage of individual cells decreases significantly from 100% to 36.3% to 24.5% to 17.3% for 0.5% (w/v) sodium alginate, while the percentage of the cells forming small aggregates increases significantly from 0% to 51.7% to 54.4% to 54.5% and the percentage of cells forming large aggregates also increases from 0% to 12% to 21.1% to 28.3%. It is noted that at the 15 min printing time, only 17.2% of cells still exist as individual cells without aggregation with other cells, leaving 82.8% of the cells to form cell aggregates. This observation indicates the significant challenge of the cell aggregation in inkjet-based bioprinting. Between 5 and 15 min of printing time, the percentage of individual cells continues to decrease while the percentage of the cells forming cell aggregates continues to increase. However, the percentage of the cells forming small aggregates only increases from 49.7% to 54.5%, while the percentage of the cells forming large aggregates increases significantly from 12% to 28.3%. This indicates that more cells tend to form large aggregates instead of small aggregates, which is mainly due to a significant increase of the cell concentration at the long printing time. More and more cells form large cell aggregates at the bottom resulting in a

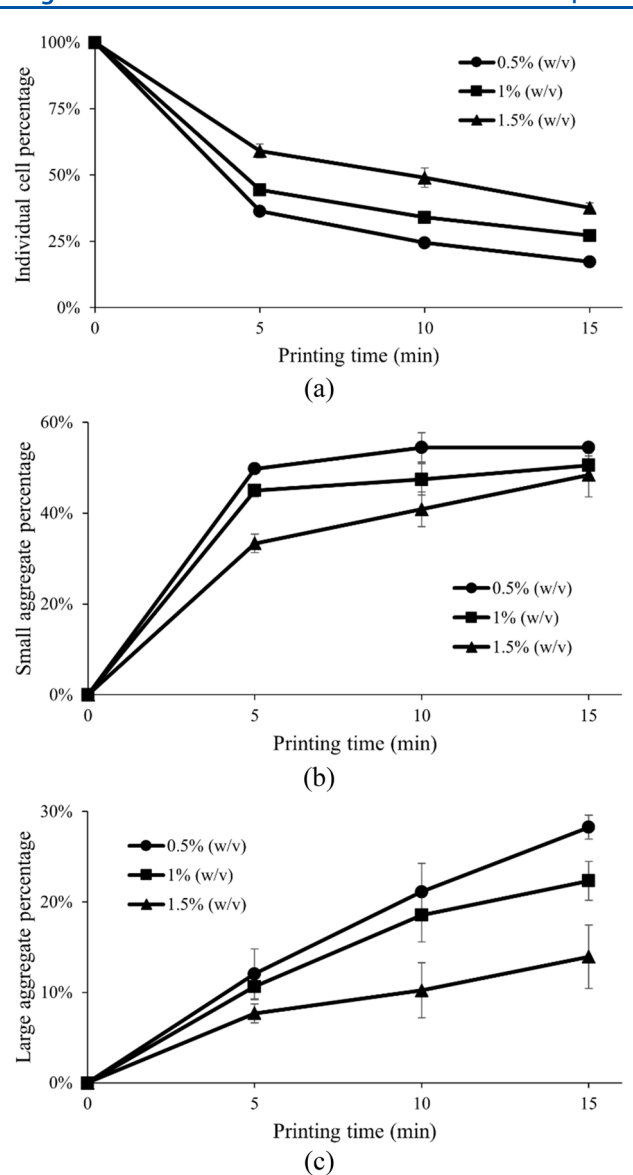


Figure 4. Effect of printing time on cell aggregation percentage using bioink containing different sodium alginate concentrations: (a) 0.5%, (b) 1%, and (c) 1.5% (w/v).

significant increase of bottom cell concentration. In other areas, the local cell concentration only increases a little, since most cells adhere to form large aggregates. In addition, as polymer concentration increases, the cell aggregation is suppressed. For example, at 15 min printing time, the percentages of the individual cells are 17.3%, 27.1%, and 37.7% for 0.5%, 1%, and 1.5% (w/v) sodium alginate, respectively. The percentages of the cells forming small aggregates are 54.5%, 50.5%, and 48.3%, and the percentages of the cells forming large aggregates are 28.3%, 22.3%, and 13.9% for 0.5%, 1%, and 1.5% (w/v) sodium alginate, respectively. This is mainly due to different cell sedimentation velocities for different sodium alginate concentrations. As sodium alginate concentration increases, the buoyant force provided by the bioink is enhanced causing the decrease of the cell sedimentation velocity. Slow cell sedimentation velocity results in a lower increase rate of the cell concentration. Therefore, it requires more time for the cells to be close enough to form cell aggregates through cell-cell interaction.

Cell aggregation is a crucial problem in inkjet-based bioprinting, especially for bioink with a low polymer concentration. For 0.5% (w/v) sodium alginate, the maximum cell aggregate observed contains 18 cells at 15 min printing time, and this number increases to around 30 cells at 30 min printing time. It is noted that when the cell aggregates are larger and larger, it becomes more and more difficult to precisely count the cell number. It is almost impossible to count how many cells are in the huge cell aggregate blocking the nozzle shown in Figure 3.

3.2. Effect of Cell Aggregation on Droplet Formation Process. It is critical to maintain a stable droplet formation process to ensure the printing performance during inkjet-based bioprinting. In inkjet-based bioprinting, the bioink is ejected out from the inkjet nozzle orifice to form a ligament that subsequently breaks up into one or several cell-laden droplets. As printing proceeds, the cells suspended within the bioink sediment result in nonuniform local cell concentration. The cell aggregates are formed due to a significant increase of the bottom cell concentration, which significantly affects the reliability of the printing process. Therefore, it is critical to understand how the cell aggregation affects the droplet formation process during inkjet-based bioprinting. Specifically, three key parameters are selected to quantify the droplet formation process, including the ligament length, breakup time, and droplet velocity.

The cell sedimentation and aggregation process are separated into two steps depending on the printing time. At a short printing time, the cells suspended within the bioink sediment, because the buoyant force is smaller than the gravitational force. The local cell concentration increases, which significantly affects the bioink properties. Specifically, with the increase of cell concentration, the storage modulus G'representing the elastic effect increases mainly due to interparticle contact and interaction. 50 The increase of the storage modulus is not pronounced, because the bioink has a relatively low volume fraction, and the interparticle contact and interaction are not significant. Moreover, as cell concentration increases, the loss modulus G" increases, demonstrating an increase in hydrodynamic energy dissipation due to the distortion of velocity field in the vicinity of each particle.<sup>50</sup> In addition, the surface tension decreases slightly as cell concentration increases. The suspended cells tend to be adsorbed to the interface, which is the most energy-favorable position. The internal energy decreases and the entropy increases, resulting in a decrease in the interfacial tension.<sup>60</sup> At a long printing time, the cells become close enough, and the cell-cell interaction force drives the cells to adhere and form different sizes of cell aggregates. Since cell aggregates are not easily adsorbed to the interface, the surface tension increases. Furthermore, cell aggregation results in a decrease of the bioink viscosity mainly due to high polydispersity.<sup>61</sup> To summarize, at the short printing time, the cell concentration increase is dominant, resulting in an increase of the viscous and elastic effects and decrease of the surface tension. At a long printing time, the cell aggregation is dominant, resulting in a decrease of the viscous effect and increase of the surface tension. During droplet formation, the total energy is transformed into several energy forms including surface energy, viscous dissipation energy, elastic energy, and kinetic energy used to generate the cell-laden droplets.<sup>50</sup> The bioink properties significantly affect the ligament length, breakup time, and droplet velocity. Generally speaking, at a short

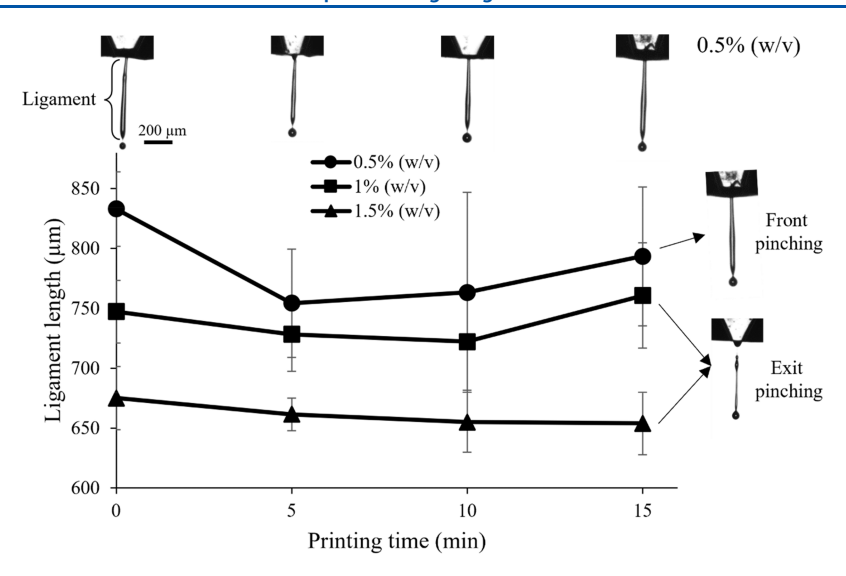


Figure 5. Effect of the printing time/cell aggregation on the ligament length during inkjet-based bioprinting of bioink with different polymer concentrations.

printing time, both the viscous and elastic effects are strengthened, and more energies are consumed for the viscous dissipation and elastic energy. The remaining kinetic energy is smaller, which causes a shorter ligament length at pinch-off and a smaller droplet velocity. 62,63 In addition, the enhanced elastic and viscous effects delay the ligament thinning and pinch-off, and the breakup time increases.<sup>64</sup> At a long printing time, the bioink viscosity decreases, resulting in reduced energy dissipation. The remaining kinetic energy used for generating the cell-laden droplets is larger, resulting in a greater volume of the ejected bioink, elongation of the ligament length, and an increase of droplet velocity. Moreover, the bioink surface tension increases due to the cell aggregation. The ligament thinning and pinch-off process is faster, and the breakup time is shorter, since the ligament thinning and pinch-off process is mainly controlled by the surface tension and capillary stress.

Figure 5 representatively compares the ligament lengths using different sodium alginate concentration-based bioink and at different printing times. The top inserted figures illustrate the change in the ligament length while ejecting the bioink containing 0.5% (w/v) sodium alginate at different printing times, and the side inserted figures compare the different pinch-off behaviors using different polymer concentrations. The viscosities of the bioink containing different concentrations of sodium alginate are measured at high shear rates at different printing times using a viscometer (Anton Paar MCR92, Anton Paar, USA). As the printing time increases from 0 to 5 to 10 to 15 min, the viscosity of the bioink containing 0.5% (w/v) sodium alginate changes from 3.8  $\pm$  0.1 to 4.5  $\pm$  0.2 to 4.4  $\pm$  0.1 to 4  $\pm$  0.2 cP, while those values change from 7.5  $\pm$  0.3 to 8  $\pm$  0.3 to 8.2  $\pm$  0.1 to 7.6  $\pm$  0.4 cP and from 15.5  $\pm$  0.4 to 15.9  $\pm$  0.2 to 16.1  $\pm$  0.3 to 16.1  $\pm$  0.2 cP for 1% (w/v) and 1.5% (w/v) sodium alginate, respectively. At short printing times, both the cell concentration and bioink viscosity increase, which is mainly caused by the cell sedimentation. The viscous dissipation increases, resulting in a shorter ligament length at 5 min printing time compared to 0 min. At long printing times, the cells accumulate at the reservoir bottom, facilitating cell aggregates due to the interaction of cells. The decrease of the viscosity of the bioink decreases causes the increase of the ligament length at a

printing time of 5-15 min. Figure 5 also shows how the printing time and cell aggregation affect the ligament length during inkjet-based bioprinting of the bioink with different polymer concentrations. The cell aggregation effect is achieved through adjusting the printing time. It clearly shows that the ligament lengths of 0.5% and 1% (w/v) sodium alginate decrease first and then increase with the printing time and cell aggregation, while that slightly decreases for 1.5% (w/v) sodium alginate. Specifically, for 0.5% (w/v) sodium alginate, the ligament length decreases from 833 to 754  $\mu$ m with the printing time increasing from 0 to 5 min. Then, it increases from 754 to 763 to 793  $\mu$ m with a printing time increase from 5 to 10 to 15 min. For 1% (w/v) sodium alginate, the ligament length decreases from 747 to 728 to 722 µm with a printing time increase from 0 to 5 to 10 min. Then it increases from 722 to 761  $\mu$ m with a printing time increase from 10 to 15 min. For 1.5% (w/v) sodium alginate, the ligament length monotonically decreases from 693 to 661 to 654 to 653  $\mu m$ with a printing time increase from 0 to 5 to 10 to 15 min.

Figure 6a demonstrates the effect of printing time and cell aggregation on the ligament breakup time during inkjet-based bioprinting. Obviously, the ligament breakup time increases first and then decreases. Specifically, for 0.5% (w/v) sodium alginate-based bioink, the ligament breakup time increases from 160 to 187  $\mu$ s with a printing time increase from 0 to 5 min. Then it decreases from 187 to 173 to 143  $\mu m$  with a printing time increase from 5 to 10 to 15 min. For 1% (w/v) sodium alginate, the ligament breakup time increases from 187 to 193 to 200  $\mu$ s with a printing time increase from 0 to 5 to 10 min. Then, it increases from 200 to 183  $\mu$ s with a printing time increase from 10 to 15 min. For 1.5% (w/v) sodium alginatebased bioink, the ligament breakup time increases from 200 to 210 to 220 µs with a printing time increase from 0 to 5 to 10 min. Then it decreases from 220 to 217  $\mu$ s with a printing time increase from 10 to 15 min. It is noted that the maximum breakup time of 0.5% (w/v) sodium alginate appears at 5 min printing time and 10 min printing time for the other two sodium alginate concentrations. Figure 5 demonstrates that the pinch-off location for 0.5% (w/v) sodium alginate is close to the forming droplet considered as front pinching.<sup>50</sup> The mechanism of front pinching is mediated by the balance of

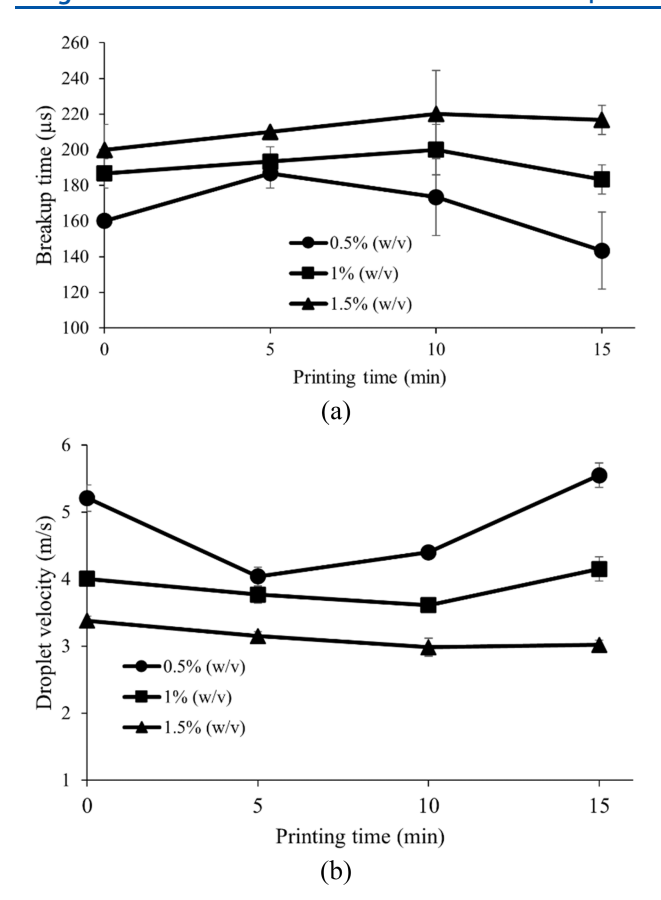


**Figure 6.** Changes in (a) breakup time and (b) droplet velocity versus printing time.

inertial force and capillary force. At 5 min printing time, the effect of the local cell concentration increase is dominant compared to the cell aggregation effect. When the local cell concentration increases, more cells are adsorbed to the interface, resulting in a reduced total free energy.<sup>50</sup> The surface tension decreases, and the ligament thinning driven by the surface tension becomes slower, resulting in an increase of the breakup time. At 5 min printing time, the cell aggregation effect is dominant compared to the effect of local cell concentration increase. Most cells adhere to form cell aggregates which are not easily adsorbed to the interface. The surface tension increases and drives the jet breakup faster. However, for 1% and 1.5% (w/v) sodium alginate, the pinchoff location is close to the nozzle orifice considered as exit pinching.<sup>50</sup> The mechanism of the exit pinch is mediated by the balance of elastic force and capillary force. For the bioink containing 1% (w/v) and 1.5% (w/v) sodium alginate, the maximum breakup time occurs at 10 min printing time, indicating the dominant effect of the local cell concentration increase before 10 min and the dominant effect of the cell aggregation after 10 min. Figure 6b demonstrates the effect of the printing time and cell aggregation on the droplet velocity during inkjet-based bioprinting. It is seen that the droplet velocity follows a similar trend like the ligament length. For 0.5% (w/v) sodium alginate, the droplet velocity decreases from 5.2 to 4 m/within the first 5 min of printing time. Then, it increases from 4 to 4.3 to 5.5 m/s with a printing time increase from 5 to 10 to 15 min. For 1% (w/v) sodium alginate, the droplet velocity decreases from 4 to 3.8 to 3.6 m/s with a printing time increase from 0 to 5 to 10 min. Then it increases

from 3.6 to 4.1 m/s with a printing time increase from 10 to 15 min. For 1.5% (w/v) sodium alginate, the droplet velocity monotonically decreases from 3.3 to 3.1 to 3 to 3 m/s with a printing time increase from 0 to 5 to 10 to 15 min.

**3.3.** Cell Aggregation Effect on Post-Printing Cell Distribution. After the pinch-off, the ligament subsequently breaks up into one or several cell-laden droplets. These droplets are accurately deposited onto the substrate containing the 2% (w/v) calcium chloride solution. Once contacting with the calcium chloride solution, the cell-laden droplets are crosslinked into the microspheres with the cells encapsulated. During inkjet-based bioprinting, the cells suspended within the bioink sediment, significantly affecting the local cell concentration and the cell aggregation. This section quantitatively investigates how the postprinting cell distribution changes with the printing time.

Figure 7 shows the effect of the printing time and cell aggregation on the diameter of the microspheres using

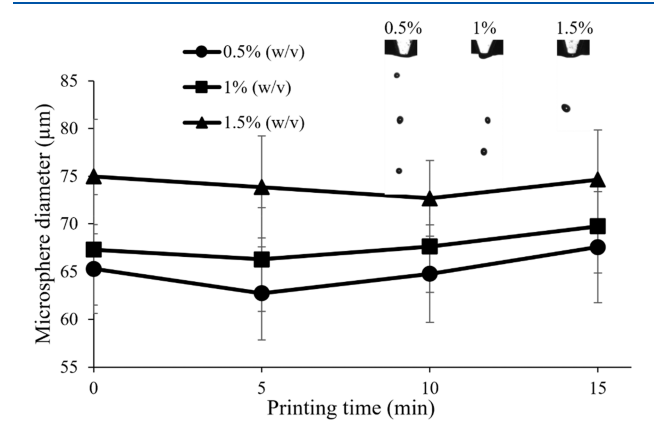


Figure 7. Microsphere diameters formed with different sodium alginate concentrations and after different printing times.

different sodium alginate concentration-based bioinks. A total of 50 microspheres are randomly chosen to characterize the average diameter of the microspheres under each condition. The inserted figures in Figure 7 compare the formed ligament during ejection using the bioink containing 0.5%, 1%, and 1.5% (w/v) sodium alginate. Figure 7 clearly shows that the microsphere diameter decreases first and then increases with the printing time and cell aggregation. Specifically, for 0.5% (w/v) sodium alginate, the microsphere diameter decreases from 65 to 63  $\mu$ m with a printing time increase from 0 to 5 min. Then, it increases from 63 to 65 to 68  $\mu$ m with a printing time increase from 5 to 10 to 15 min. For 1% (w/v) sodium alginate, the microsphere diameter decreases from 67 to 66  $\mu$ m with a printing time increase from 0 to 5 min. Then, it increases from 66 to 67 to 69  $\mu m$  with a printing time increase from 5 to 10 to 15 min. For 1.5% (w/v) sodium alginate, the microsphere diameter decreases from 75 to 74 to 73  $\mu$ m with a printing time increase from 0 to 5 to 10 min. Then it increases from 73 to 75  $\mu$ m with a printing time increase from 10 to 15 min. This observation is similar to the effect of the printing time and cell aggregation on the ligament length. At a short printing time, the local cell concentration increases due to the cell sedimentation, causing an increase of the bioink viscosity and decrease of the microsphere size. At long printing times, the cells adhere to form cell aggregates and the local viscosity

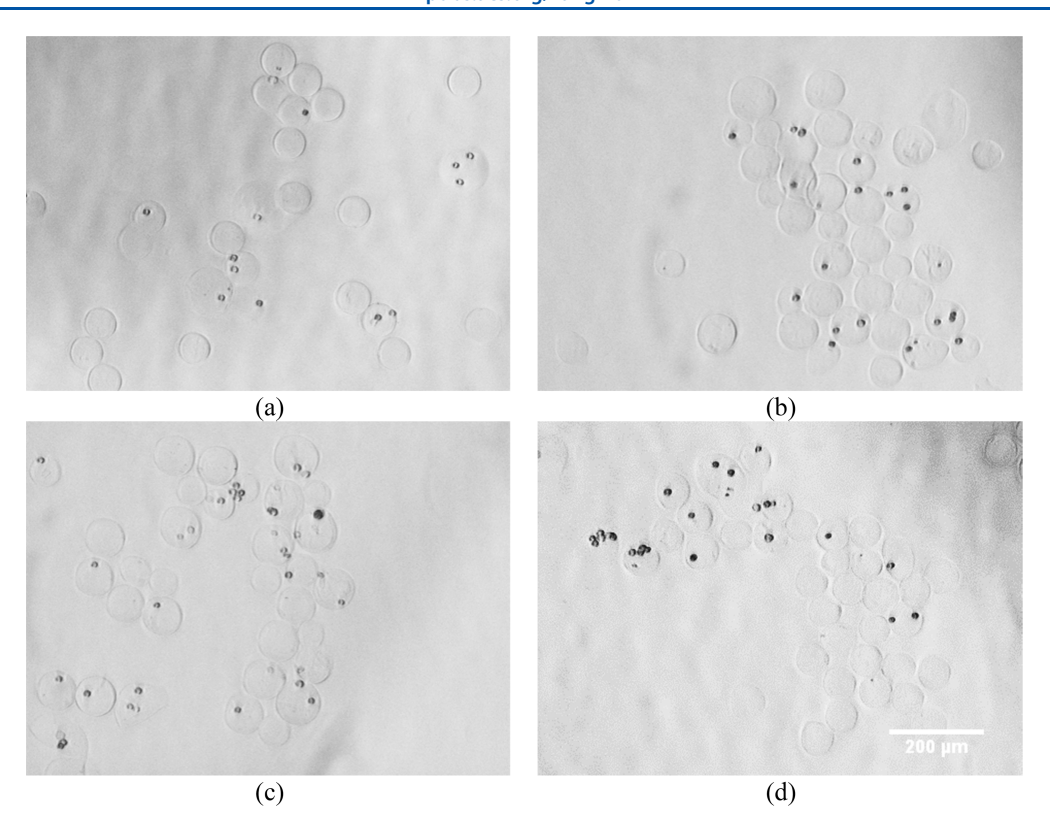


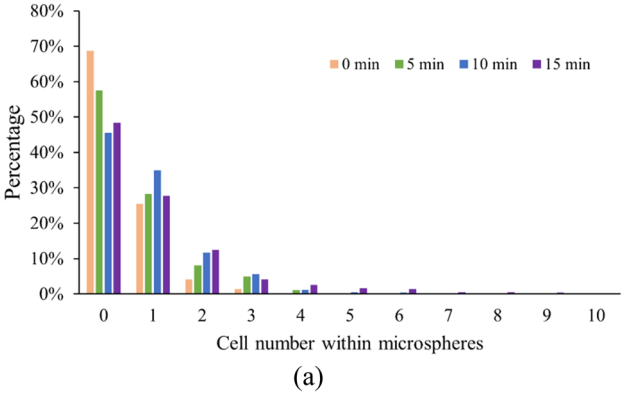
Figure 8. Representative images of microspheres with cells encapsulated using 1% (w/v) sodium alginate at a printing time of (a) 0 min, (b) 5 min, (c) 10 min, and (d) 15 min. All four figures share the same scale bar.

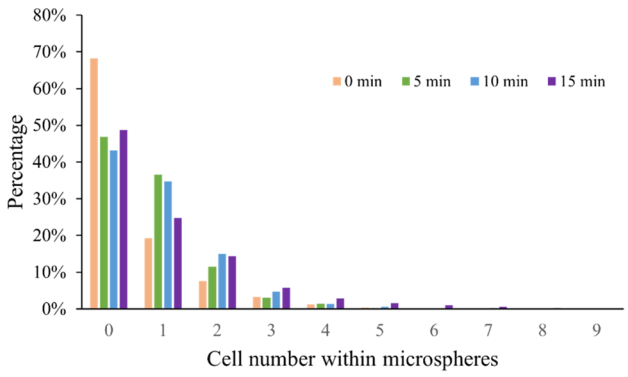
of the bioink decreases, which makes the ligament longer and the microsphere larger.

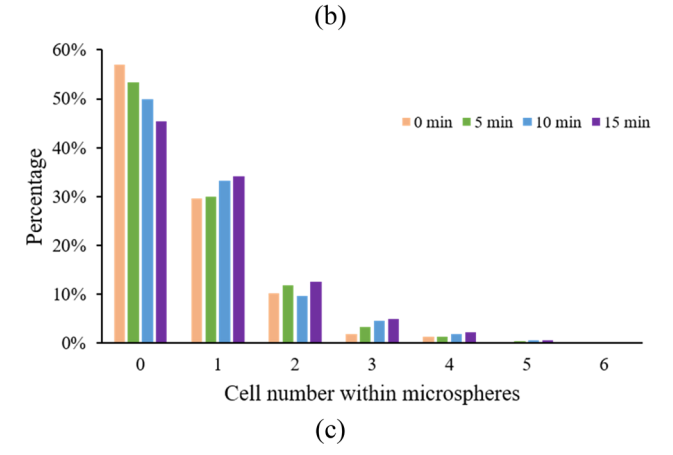
Figure 8 shows representative images of microspheres with cells encapsulated during inkjet-based bioprinting of the bioink containing 1% (w/v) sodium alginate at different printing times. At a printing time of 0 min, some microspheres have no cells encapsulated, and some have one or two or three cells capsulated. The encapsulated cells are separate from each other without cell aggregation. At 5 min printing time, more cells are encapsulated, and one microsphere has three cells, including one individual cell and one aggregate with two cells. At 10 min printing time, the majority of the microspheres have cells encapsulated, and more cell aggregates are observed. One microsphere has a small aggregate containing four cells. At a printing time of 15 min, many microspheres have no cells encapsulated, indicating nonuniform cell distribution due to cell aggregation. Large cell aggregates are observed, and one microsphere has a large aggregate containing six cells. During the experiments, it is observed that the cell aggregation phenomenon is more significant for the bioink composed of lower concentrations of sodium alginate, because the cell sedimentation velocity and the accumulation rate of the cells are faster. For example, the maximum cell aggregate observed using 0.5% (w/v) sodium alginate contains 10 cells, while that for 1.5% (w/v) sodium alginate is 6.

Figure 9 shows the distribution of cells within the formed microspheres with different sodium alginate concentrations and at different printing times. Specifically, Figure 9a,b,c demonstrate the cell distribution using the bioink containing 0.5%, 1%, and 1.5% (w/v) sodium alginate, respectively. Under each condition, 1000 random microspheres are chosen to quantify the cell distribution within the microspheres. Obviously, for 0.5% (w/v) sodium alginate shown in Figure

9a, the maximum number of cells within one microsphere increases significantly 3 to 4 to 6 to 10 as the printing time increases from 0 to 5 to 10 to 15 min, which is mainly due to the continuous increase in the cell concentration and the formation of cell aggregates. Typically, one microsphere containing at least five cells is mainly due to the formation of large cell aggregates. At 10 min of printing time, the large cell aggregates are observed containing at least five cells. With a printing time increase from 10 to 15 min, the percentage of the large cell aggregates increases significantly from 0.9% to 4.7%. In addition, the percentage of the microspheres without cells decreases from 68.7% to 57.5% to 45.6% with a printing time increase from 0 to 5 to 10 min. This is mainly due to the increase of the local cell concentration caused by the cell sedimentation. However, from the printing time of 10 to 15 min, the percentage of the microspheres with no cells encapsulated increases from 45.6% to 48.4%. The main reason is the decrease of the local individual cell concentration due to the cell aggregation. For 1% and 1.5% (w/v) sodium alginate shown in Figure 9b and c, with a printing time increase from 0 to 5 to 10 to 15 min, the maximum number of cells within one microsphere increases from 5 to 7 to 8 to 9 using 1% (w/v) sodium alginate, while that only changes from 5 to 5 to 6 to 6 for 1.5% (w/v) sodium alginate. This is because a higher polymer concentration reduces the cell sedimentation velocity and restricts the formation of cell aggregates. In addition, for 1% (w/v) sodium alginate, the percentage of the microspheres without cells decreases from 68.3% to 46.9% to 43.3% with a printing time increase from 0 to 5 to 10 min due to the increase in local cell concentration caused by the cell sedimentation. With the printing time further increasing from 10 to 15 min, the percentage of the microspheres without cells increases from 43.3% to 48.7% due to the







**Figure 9.** Cell distribution within the microspheres using the bioink containing (a) 0.5% (w/v), (b) 1% (w/v), and (c) 1.5% (w/v) sodium alginate at different printing times.

dominant effect of the cell aggregation. This observation is analogous to 0.5% (w/v) sodium alginate. However, for 1.5% (w/v) sodium alginate, the percentage of the microspheres without cells decreases monotonically from 57.1% to 53.4% to 50% to 45.5% with a printing time increase from 0 to 5 to 10 to 15 min due to the dominant cell concentration increase caused by the cell sedimentation. The percentage of the microspheres containing large cell aggregates at the 15 min printing time is 4.7%, 3.6%, and 0.8% for 0.5%, 1%, and 1.5% (w/v) sodium alginate, respectively. This indicates that high polymer concentrations significantly restrict the formation of large cell aggregates.

Figure 10 compares the mean cell number within the microspheres using the bioink containing different sodium alginate concentrations and at different printing time. Clearly, for all three selected sodium alginate concentrations, the mean cell number increases nearly linearly with the printing time for

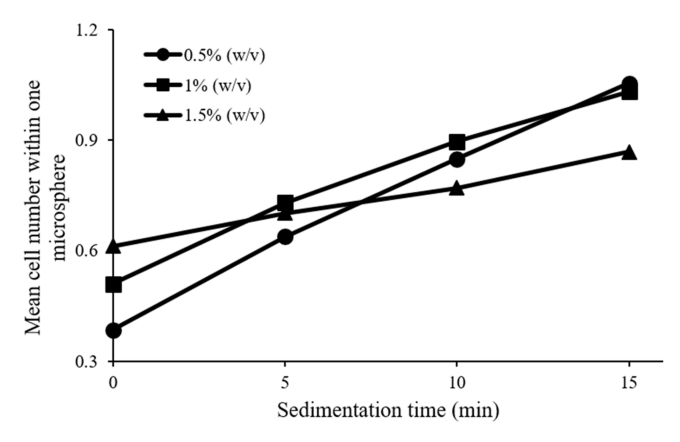


Figure 10. Mean cell number within one microsphere.

the bioink. Specifically, for 0.5% (w/v) sodium alginate, the mean cell number within the microspheres increases significantly from 0.38 to 0.64 to 0.85 to 1.05 as the printing time increases from 0 to 5 to 10 to 15 min, while those values increase significantly from 0.51 to 0.73 to 0.9 to 1.03 and from 0.61 to 0.7 to 0.77 to 0.86 for 1% (w/v) and 1.5% (w/v) sodium alginate, respectively. The observations indicate continuous and stable increase of the local cell concentration due to the cell sedimentation with the printing time. It is also noted that the increased rate of the mean cell number is highest using the bioink containing the lowest polymer concentration of 0.5% (w/v), which is mainly because of the fastest cell sedimentation velocity.

#### 4. CONCLUSIONS

3D bioprinting has been intensively utilized in various biomedical applications. As a key element in 3D bioprinting, the bioink contains biological materials and living cells. When the buoyant is unable to counteract the gravitational force, cell sedimentation occurs, resulting in the accumulation of cells at the bioink reservoir bottom. Once the cells are close, the formation of cell aggregates are facilitated under the interaction of cells, which has a significant effect on the printing reliability. In this study, a typical cell concentration of  $1.5 \times 10^6$  cells/mL is selected, and a severe cell aggregation phenomenon has been observed only within 15 min of printing time. Higher cell concentrations will facilitate the formation of cell aggregates significantly affecting the printing performance. In addition, cell aggregates, especially large sized cell aggregates composed of multiple individual cells, may have an adverse effect on cell viability since the exterior cells may block the nutrient and oxygen exchange of the interior cells reducing cell viability. This paper mainly studies cell aggregation and its effects on the droplet formation process during inkjet bioprinting and postprinting cell distribution. The major conclusions of this study are as follows:

(1) With the printing time increase from 0 to 15 min, the percentage of individual cells decreases significantly from 100% to 17.3% for 0.5% (w/v) sodium alginate. On the contrary, the percentage of the cells forming small aggregates and large aggregates increases significantly from 0% to 54.5% and from 0% to 28.3%, respectively. This observation indicates the significant challenge of the cell aggregation during inkjet-based bioprinting. In addition, as the polymer concentration increases, the cell aggregation is suppressed mainly due to reduced cell sedimentation velocity.

- (2) As the printing time and cell aggregation increase, the ligament length and droplet velocity generally decrease first and then increase. At a short printing time, the bioink viscous effect increases due to the local cell concentration increase caused by the cell sedimentation, while at a long printing time, the bioink's viscous effect decreases due to the dominant cell aggregation. The maximum breakup time of front pinching is at 5 min printing time for 0.5% (w/v) sodium alginate, while the maximum breakup time of exit pinching is at 10 min printing time for 1% and 1.5% (w/v) sodium alginate. For 1.5% (w/v) sodium alginate, the maximum breakup time at 10 min printing time indicates the dominant effect of the local cell concentration increase before 10 min and decrease of the elastic force due to cell aggregation after 10 min. With a longer printing time and more severe cell aggregation, the droplet formation process will be continuously affected until the nozzle is clogged by a large cell aggregate whose size is comparable to the nozzle.
- (3) As the printing time increases from 0 to 5 to 10 to 15 min, the maximum number of cells encapsulated within one microsphere increases significantly from 3 to 10, from 5 to 9, and from 5 to 6 for 0.5%, 1%, and 1.5% ( $\rm w/v$ ) sodium alginate-based bioink, respectively. The mean cell number increases nearly linearly with the printing time. The increased rate of the mean cell number is the highest using the bioink containing the lowest polymer concentration of 0.5% ( $\rm w/v$ ), because the lower polymer concentration results in a higher cell sedimentation velocity promoting the cell sedimentation and aggregation.

Future work may include the development of an effective approach to mitigate cell sedimentation and aggregation to improve the printing performance in 3D bioprinting.

# AUTHOR INFORMATION

# **Corresponding Author**

Changxue Xu — Department of Industrial, Manufacturing, and Systems Engineering, Texas Tech University, Lubbock, Texas 79409, United States; orcid.org/0000-0002-5323-595X; Phone: 806-834-6014; Email: changxue.xu@ttu.edu

#### Authors

Heqi Xu — Department of Industrial, Manufacturing, and Systems Engineering, Texas Tech University, Lubbock, Texas 79409, United States; The State Key Laboratory of Fluid Power and Mechatronic Systems, School of Mechanical Engineering, Zhejiang University, Hangzhou 310028, China; orcid.org/0000-0002-1667-1226

Jiachen Liu – Department of Industrial, Manufacturing, and Systems Engineering, Texas Tech University, Lubbock, Texas 79409, United States

Md Shahriar — Department of Industrial, Manufacturing, and Systems Engineering, Texas Tech University, Lubbock, Texas 79409, United States; orcid.org/0000-0003-4895-2601

Complete contact information is available at: https://pubs.acs.org/10.1021/acs.langmuir.2c02817

#### Notes

The authors declare no competing financial interest.

#### ACKNOWLEDGMENTS

This work was partially supported by the National Science Foundation (NSF; No. CMMI-1762282).

#### REFERENCES

- (1) Bhattacharyya, A.; Janarthanan, G.; Noh, I. Nano-biomaterials for designing functional bioinks towards complex tissue and organ regeneration in 3D bioprinting. *Addit. Manuf.* **2021**, *37*, 101639.
- (2) Aljohani, W.; Ullah, M. W.; Zhang, X.; Yang, G. Bioprinting and its applications in tissue engineering and regenerative medicine. *Int. J. Biol. Macromol.* **2018**, *107*, 261–275.
- (3) Foyt, D. A.; Norman, M. D.; Yu, T. T.; Gentleman, E. Exploiting advanced hydrogel technologies to address key challenges in regenerative medicine. *Adv. Healthc. Mater.* **2018**, *7*, 1700939.
- (4) Mandrycky, C.; Wang, Z.; Kim, K.; Kim, D.-H. 3D bioprinting for engineering complex tissues. *Biotechnol. Adv.* **2016**, 34, 422–434.
- (5) Cui, X.; Breitenkamp, K.; Finn, M.; Lotz, M.; D'Lima, D. D. Direct human cartilage repair using three-dimensional bioprinting technology. *Tissue Eng. Part A* **2012**, *18*, 1304–1312.
- (6) Xu, T.; Jin, J.; Gregory, C.; Hickman, J. J.; Boland, T. Inkjet printing of viable mammalian cells. *Biomaterials*. **2005**, *26*, 93–99.
- (7) Krishnamoorthy, S.; Zhang, Z.; Xu, C. Biofabrication of three-dimensional cellular structures based on gelatin methacrylate—alginate interpenetrating network hydrogel. *J. Biomater. Appl.* **2019**, 33, 1105—1117.
- (8) Peltola, S. M.; Melchels, F. P.; Grijpma, D. W.; Kellomäki, M. A review of rapid prototyping techniques for tissue engineering purposes. *Ann. Med.* **2008**, *40*, 268–280.
- (9) Chang, R.; Nam, J.; Sun, W. Effects of dispensing pressure and nozzle diameter on cell survival from solid freeform fabrication—based direct cell writing. *Tissue Eng. Part A* **2008**, *14*, 41–48.
- (10) Guillotin, B.; Souquet, A.; Catros, S.; Duocastella, M.; Pippenger, B.; Bellance, S.; Bareille, R.; Remy, M.; Bordenave, L.; Amedee, J.; Guillemot, F. Laser assisted bioprinting of engineered tissue with high cell density and microscale organization. *Biomaterials*. **2010**, *31*, 7250–7256.
- (11) Zhang, Z.; Chai, W.; Xiong, R.; Zhou, L.; Huang, Y. Printing-induced cell injury evaluation during laser printing of 3T3 mouse fibroblasts. *Biofabrication*. **2017**, *9*, 025038.
- (12) Kattamis, N. T.; Purnick, P. E.; Weiss, R.; Arnold, C. B. Thick film laser induced forward transfer for deposition of thermally and mechanically sensitive materials. *Appl. Phys. Lett.* **2007**, *91*, 171120.
- (13) Li, Y.; Mao, Q.; Yin, J.; Wang, Y.; Fu, J.; Huang, Y. Theoretical prediction and experimental validation of the digital light processing (DLP) working curve for photocurable materials. *Addit. Manuf.* **2021**, 37, 101716.
- (14) Kačarević, Ż. P.; Rider, P. M.; Alkildani, S.; Retnasingh, S.; Smeets, R.; Jung, O.; Ivanišević, Z.; Barbeck, M. An introduction to 3D bioprinting: possibilities, challenges and future aspects. *Materials*. **2018**, *11*, 2199.
- (15) Zennifer, A.; Manivannan, S.; Sethuraman, S.; Kumbar, S. G.; Sundaramurthi, D. 3D bioprinting and photocrosslinking: emerging strategies & future perspectives. *Mater. Sci. Eng. C* **2022**, *134*, 112576.
- (16) Zhao, D.; Zhou, H.; Wang, Y.; Yin, J.; Huang, Y. Drop-on-demand (DOD) inkjet dynamics of printing viscoelastic conductive ink. Addit. Manuf. 2021, 48, 102451.
- (17) Wu, D.; Xu, C. Predictive modeling of droplet formation processes in inkjet-based bioprinting. *J. Manuf. Sci. Eng.* **2018**, *140*, 101007.
- (18) Gao, G.; Yonezawa, T.; Hubbell, K.; Dai, G.; Cui, X. Inkjetbioprinted acrylated peptides and PEG hydrogel with human mesenchymal stem cells promote robust bone and cartilage formation with minimal printhead clogging. *Biotechnol. J.* **2015**, *10*, 1568–1577.
- (19) Benning, L.; Gutzweiler, L.; Tröndle, K.; Riba, J.; Zengerle, R.; Koltay, P.; Zimmermann, S.; Stark, G. B.; Finkenzeller, G. Assessment of hydrogels for bioprinting of endothelial cells. *J. Biomed. Mater. Res.* A **2018**, *106*, 935–947.
- (20) Takagi, D.; Lin, W.; Matsumoto, T.; Yaginuma, H.; Hemmi, N.; Hatada, S.; Seo, M. High-precision three-dimensional inkjet technology for live cell bioprinting. *Int. J. Bioprinting.* **2019**, *5*, 27.
- (21) Gao, G.; Schilling, A. F.; Hubbell, K.; Yonezawa, T.; Truong, D.; Hong, Y.; Dai, G.; Cui, X. Improved properties of bone and cartilage tissue from 3D inkjet-bioprinted human mesenchymal stem

- cells by simultaneous deposition and photocrosslinking in PEG-GelMA. *Biotechnol. Lett.* **2015**, *37*, 2349–2355.
- (22) Skardal, A.; Mack, D.; Kapetanovic, E.; Atala, A.; Jackson, J. D.; Yoo, J.; Soker, S. Bioprinted amniotic fluid-derived stem cells accelerate healing of large skin wounds. *Stem Cells Transl. Med.* **2012**, *1*, 792–802.
- (23) Cui, X.; Gao, G.; Yonezawa, T.; Dai, G. Human cartilage tissue fabrication using three-dimensional inkjet printing technology. *J. Vis. Exp.* **2014**, 88, e51294.
- (24) Xu, C.; Zhang, Z.; Christensen, K.; Huang, Y.; Fu, J.; Markwald, R. R. Freeform vertical and horizontal fabrication of alginate-based vascular-like tubular constructs using inkjetting. *J. Manuf. Sci. Eng.* **2014**, *136*, 061020.
- (25) Jiao, T.; Lian, Q.; Zhao, T.; Wang, H.; Li, D. Preparation, mechanical and biological properties of inkjet printed alginate/gelatin hydrogel. *J. Bionic Eng.* **2021**, *18*, 574–583.
- (26) Gopinathan, J.; Noh, I. Recent trends in bioinks for 3D printing. *Biomater. Res.* **2018**, 22, 11.
- (27) Park, J.; Lee, S. J.; Chung, S.; Lee, J. H.; Kim, W. D.; Lee, J. Y.; Park, S. A. Cell-laden 3D bioprinting hydrogel matrix depending on different compositions for soft tissue engineering: characterization and evaluation. *Mater. Sci. Eng. C* **2017**, *71*, 678–684.
- (28) Yin, J.; Zhao, D.; Liu, J. Trends on physical understanding of bioink printability. *Bio-Des. Manuf.* **2019**, *2*, 50–54.
- (29) Unagolla, J. M.; Jayasuriya, A. C. Hydrogel-based 3D bioprinting: A comprehensive review on cell-laden hydrogels, bioink formulations, and future perspectives. *Appl. Mater. Today.* **2020**, *18*, 100479.
- (30) Zhang, T.; Zhao, W.; Xiahou, Z.; Wang, X.; Zhang, K.; Yin, J. Bioink design for extrusion-based bioprinting. *Appl. Mater. Today.* **2021**, 25, 101227.
- (31) Yang, X.; Lu, Z.; Wu, H.; Li, W.; Zheng, L.; Zhao, J. Collagenalginate as bioink for three-dimensional (3D) cell printing based cartilage tissue engineering. *Mater. Sci. Eng. C* **2018**, 83, 195–201.
- (32) Axpe, E.; Oyen, M. L. Applications of alginate-based bioinks in 3D bioprinting. *Int. J. Mol. Sci.* **2016**, *17*, 1976.
- (33) Ruberu, K.; Senadeera, M.; Rana, S.; Gupta, S.; Chung, J.; Yue, Z.; Venkatesh, S.; Wallace, G. Coupling machine learning with 3D bioprinting to fast track optimization of extrusion printing. *Appl. Mater. Today.* **2021**, 22, 100914.
- (34) Narayanan, L. K.; Huebner, P.; Fisher, M. B.; Spang, J. T.; Starly, B.; Shirwaiker, R. A. 3D-bioprinting of polylactic acid (PLA) nanofiber—alginate hydrogel bioink containing human adiposederived stem cells. *ACS Biomater. Sci. Eng.* **2016**, *2*, 1732–1742.
- (35) Yu, H.; Tay, C. Y.; Pal, M.; Leong, W. S.; Li, H.; Li, H.; Wen, F.; Leong, D. T.; Tan, L. P. A bio-inspired platform to modulate myogenic differentiation of human mesenchymal stem cells through focal adhesion regulation. *Adv. Healthc. Mater.* **2013**, *2*, 442–449.
- (36) Salaris, F.; Rosa, A. Construction of 3D in vitro models by bioprinting human pluripotent stem cells: challenges and opportunities. *Brain Res.* **2019**, *1723*, 146393.
- (37) Griffith, L. G.; Swartz, M. A. Capturing complex 3D tissue physiology in vitro. *Nature Rev. Mol. Cell Biol.* **2006**, *7*, 211–224.
- (38) Zhang, Z.; Jin, Y.; Yin, J.; Xu, C.; Xiong, R.; Christensen, K.; Ringeisen, B. R.; Chrisey, D. B.; Huang, Y. Evaluation of bioink printability for bioprinting applications. *Appl. Phys. Rev.* **2018**, *5*, 041304.
- (39) Liu, F.; Liu, C.; Chen, Q.; Ao, Q.; Tian, X.; Fan, J.; Tong, H.; Wang, X. Progress in organ 3D bioprinting. *Int. J. Bioprinting.* **2018**, *4*, 128.
- (40) Saunders, R. E.; Gough, J. E.; Derby, B. Delivery of human fibroblast cells by piezoelectric drop-on-demand inkjet printing. *Biomaterials.* **2008**, *29*, 193–203.
- (41) Parsa, S.; Gupta, M.; Loizeau, F.; Cheung, K. C. Effects of surfactant and gentle agitation on inkjet dispensing of living cells. *Biofabrication*. **2010**, 2, 025003.
- (42) Chahal, D.; Ahmadi, A.; Cheung, K. C. Improving piezoelectric cell printing accuracy and reliability through neutral buoyancy of suspensions. *Biotechnol. Bioeng.* **2012**, *109*, 2932–2940.

- (43) Graham, A. D.; Olof, S. N.; Burke, M. J.; Armstrong, J. P.; Mikhailova, E. A.; Nicholson, J. G.; Box, S. J.; Szele, F. G.; Perriman, A. W.; Bayley, H. High-resolution patterned cellular constructs by droplet-based 3D printing. *Sci. Rep.* **2017**, *7*, 7004.
- (44) Xu, H.; Zhang, Z.; Xu, C. Sedimentation study of bioink containing living cells. *J. Appl. Phys.* **2019**, *125*, 114901.
- (45) Xu, H.; Martinez Salazar, D. M.; Xu, C. Investigation of cell concentration change and cell aggregation due to cell Sedimentation during inkjet-Based bioprinting of cell-laden bioink. *Machines.* **2022**, *10*, 315.
- (46) Xu, H.; Martinez Salazar, D. M.; Shahriar, M.; Xu, C. Investigation and characterization of cell aggregation during and after inkjet-based bioprinting of cell-laden bioink. *J. Manuf. Sci. Eng.* **2022**, 144, 104501.
- (47) Kim, J. S.; Hong, S.; Hwang, C. Bio-ink materials for 3D bio-printing. J. Int. Soc. Simu. Surg. 2016, 3, 49–59.
- (48) Murphy, S. V.; Skardal, A.; Atala, A. Evaluation of hydrogels for bio-printing applications. *J. Biomed. Mater. Res., Part A* **2013**, *101*, 272–284.
- (49) Merceron, T. K.; Burt, M.; Seol, Y.-J.; Kang, H.-W.; Lee, S. J.; Yoo, J. J.; Atala, A. A 3D bioprinted complex structure for engineering the muscle—tendon unit. *Biofabrication*. **2015**, *7*, 035003.
- (50) Xu, C.; Zhang, M.; Huang, Y.; Ogale, A.; Fu, J.; Markwald, R. R. Study of droplet formation process during drop-on-demand inkjetting of living cell-laden bioink. *Langmuir.* **2014**, *30*, 9130–9138.
- (51) Xu, H.; Casillas, J.; Xu, C. Effects of printing conditions on cell distribution within microspheres during inkjet-based bioprinting. *AIP Adv.* **2019**, *9*, 095055.
- (52) Xu, H.; Liu, Q.; Casillas, J.; Mcanally, M.; Mubtasim, N.; Gollahon, L. S.; Wu, D.; Xu, C. Prediction of cell viability in dynamic optical projection stereolithography-based bioprinting using machine learning. *J. Intell. Manuf.* **2022**, *33*, 995–1005.
- (53) Xu, H.; Casillas, J.; Krishnamoorthy, S.; Xu, C. Effects of Irgacure 2959 and lithium phenyl-2, 4, 6-trimethylbenzoylphosphinate on cell viability, physical properties, and microstructure in 3D bioprinting of vascular-like constructs. *Biomed. Mater.* **2020**, *15*, 055021.
- (54) Li, X.; Liu, B.; Pei, B.; Chen, J.; Zhou, D.; Peng, J.; Zhang, X.; Jia, W.; Xu, T. 2020. Inkjet bioprinting of biomaterials. *Chem. Rev.* **2020**, *120*, 10793–10833.
- (55) Zhang, M.; Krishnamoorthy, S.; Song, H.; Zhang, Z.; Xu, C. Ligament flow during drop-on-demand inkjet printing of bioink containing living cells. *J. Appl. Phys.* **2017**, *121*, 124904.
- (56) Xu, C.; Chai, W.; Huang, Y.; Markwald, R. R. Scaffold-free inkjet printing of three-dimensional zigzag cellular tubes. *Biotechnol. Bioeng.* **2012**, *109*, 3152–3160.
- (57) Christensen, K.; Xu, C.; Chai, W.; Zhang, Z.; Fu, J.; Huang, Y. Freeform inkjet printing of cellular structures with bifurcations. *Biotechnol. Bioeng.* **2015**, *112*, 1047–1055.
- (58) Xu, T.; Kincaid, H.; Atala, A.; Yoo, J. J. High-throughput production of single-cell microparticles using an inkjet printing technology. *J. Manuf. Sci. Eng.* **2008**, *130*, 021017.
- (59) Xu, H.; Liu, J.; Zhang, Z.; Xu, C. Cell sedimentation during 3D bioprinting: a mini review. *Bio-Des. Manuf.* **2022**, *5*, 617–626.
- (60) Dong, L.; Johnson, D. Surface tension of charge-stabilized colloidal suspensions at the water—air interface. *Langmuir.* **2003**, *19*, 10205—10209.
- (61) Nicoud, L.; Lattuada, M.; Yates, A.; Morbidelli, M. Impact of aggregate formation on the viscosity of protein solutions. *Soft Matter.* **2015**, *11*, 5513–5522.
- (62) Jang, D.; Kim, D.; Moon, J. Influence of fluid physical properties on ink-jet printability. *Langmuir.* **2009**, 25, 2629–2635.
- (63) Yu, J.-D.; Sakai, S.; Sethian, J. A. Two-phase viscoelastic jetting. *J. Comput. Phys.* **2007**, 220, 568–585.
- (64) Anna, S. L.; McKinley, G. H. Elasto-capillary thinning and breakup of model elastic liquids. *J. Rheol.* **2001**, *45*, 115–138.